Pyrolysis and combustion of municipal solid wastes: Evaluation of synergistic effects using TGA-MS

Sanjana D. Gunasee[a,c*], Marion Carrier[b,c], Johann F. Gorgens[b], Romeela Mohee[d]

[a] Department of Chemical Engineering, University of Mauritius, Reduit, Mauritius

[b] Department of Process Engineering, Stellenbosch University, South Africa

[c] Aston University, EBRI, Bioenergy Research group, Birmingham B4 7ET, United Kingdom

[d] University of Mauritius, Reduit, Mauritius

* Corresponding author: Sanjana Gunasee; Email: san_gunasee@hotmail.com; Tel: +23057829952

Abstract

A thermogravimetric methodology was developed to investigate and semi-quantify the extent of synergistic effects during pyrolysis and combustion of municipal solid waste (MSW). Results from TGA-MS were used to compare the pyrolysis and combustion characteristics of single municipal solid waste components (polyvinyl chloride (PVC), polypropylene (PP), polystyrene (PS), branches (BR), leaves (LV), grass (GR), packaging paper (PK), hygienic paper (HP) and cardboard (CB)) and a mixture (MX) of PP, BR and CB. Samples were heated under dynamic conditions at 20°C/min from 25°C to 1000°C with the continuous record of their main evolved fragments. Synergistic effects were evaluated by comparing experimental and calculated weight losses and relative areas of MS peaks. Pyrolysis of the mixture happened in two stages, with the

release of H_2, CH_4, H_2O CO and CO_2 between 200-415°C and the release of CH_4, C_xH_y, CO and CO_2 between 415-525°C. Negative synergistic effect in the 1st stage was attributed to the presence of PP where the release of hydrocarbons and CO_2 from BR and CB was inhibited, whereas positive synergistic effects were observed during the 2nd degradation stage. In a second part of the study, synergistic effects were related to the dependency of the effective activation energy (E_α) versus the conversion (α). Higher E_αs were obtained for MX during its 1st stage of pyrolysis and lower E_αs for the 2nd stage when compared to the individual components. On the other hand, mostly positive synergistic effects were observed during the combustion of the same mixture, for which lower E_αs were recorded.

Keywords: Municipal solid wastes, TGA-MS, pyrolysis, combustion, synergy

1. Introduction

Rapid industrialization and population growth have led to an increase in generation of municipal solid wastes (MSW) to such an extent that the management of solid wastes have become a major concern in developing countries [1]. In Mauritius, solid wastes were traditionally disposed off in open dumps and uncontrolled landfill, which pose potential environmental threats and health issues [2]. At present, the waste generation rate per capita in Mauritius is higher than most developing countries [3]. Two disposal methods namely landfill and composting are currently applied, although the growth in solid waste generation and the lack of landfill space requires an alternative solid waste treatment [4]. On the other hand, with Mauritius being highly dependent on the import of petroleum to meet its requirement of energy, the government has proposed the 'Maurice Ile Durable' concept, aiming to be 65% self-sufficient in renewable energy by 2028. As such, thermochemical techniques can be applied for the treatment of MSW because they provide

an efficient solution to reduce the volume of MSW, which can be subsequently converted into recoverable energy as replacement for fossil fuels [5].

Combustion was suggested as an alternative to landfill and for the rejects of the non-compostable fraction from the composting plant [4]. Combustion is the thermal processing of solid waste by chemical oxidation with usually excess amount of air to produce a flue gas and a solid residue as products [6]. The major combustible fractions of MSW in Mauritius are paper (12 % w/w), plastic (13 %w/w) and yard waste (43 %w/w) [7]. Pyrolysis was also suggested as another alternative for the treatment of MSW as it has received much attention during recent years. Pyrolysis which is theoretically a zero-air indirect process for the thermal decomposition of solids, presents the advantage of converting MSW into several usable products such as low molecular weight gases, heavy volatiles (tar) and solid char [8,9]. The effect of heat on MSW depends on the atmosphere used. The use of combustion or pyrolysis atmosphere causes different types of reactions to happen and hence the degradation of solid wastes occurs by different pathways producing different types of products.

Efficient conversion of solid wastes to energy products, through thermochemical techniques, requires the understanding of their thermal behaviour [10]. Thermogravimetric analysis (TGA) is a preferred technique to study the kinetic behaviour of samples' thermal degradation at low heating rates although it provides limited information on products evolved and secondary reactions of thermal conversion [11]. Coupling TGA with Fourier Transform Infrared spectroscopy (FTIR) or with Mass Spectroscopy (MS) provides some information on the thermal decomposition and reaction mechanisms. For example, Singh *et al.* [12] assessed the volatile species evolved during the pyrolysis of several natural and synthetic polymers using both TGA-

FTIR and TGA-MS techniques and concluded that both techniques were capable of providing qualitative information on the volatile species evolved during pyrolysis.

Several researchers have applied TGA to study the pyrolytic [5,8,13] and combustive [14,15] characteristics of MSW, using selected individual waste components and/or mixtures. Previous studies have shown that the pyrolysis and combustion degradation stages of various biomass fuels and selected mixtures thereof were different [10, 16]. Under inert atmosphere, each material degraded in a single stage, depending on the content and composition of inorganics, while between two and three degradation stages were observed for each component under combustion conditions. In addition, thermal decomposition processes occur at lower temperatures in oxidising atmospheres as compared to pyrolysis conditions. However, there are few comparative studies on the volatiles evolved from the components of MSW during combustion and pyrolysis [12, 17, 18].

MSW is a complex mixture of different types of components. During pyrolysis and combustion of MSW, the different components do not degrade independently in the mixture and some interactions may give rise to synergies. Synergy occurring during co-pyrolysis and co-combustion is the difference between the actual experimental yield or composition of the products and the value calculated according to the ratio of the individual components in the mixture [19]. Several researchers mentioned that the mechanism of synergistic effect between plastic and biomass is still unclear [20, 21]. Besides, while many works describe the thermal behaviour of single feedstocks, few have attempted to describe the apparent activation energy of potential reactional synergies occurring during the thermal conversion of a mixture [22].

Therefore, the aim of this work is to study both pyrolysis and combustion of typical municipal wastes to gain knowledge on eventual synergistic mechanisms. To do this, we used the TGA-MS

technique and determine activation energies to quantitatively describe the extent of synergetic mechanisms and associated threshold..

2. Materials and methods

2.1 Materials

Combustible fractions from municipal solid wastes (MSW) were selected as feedstocks. In total, nine different feedstocks were classified in three main categories: plastics [polyvinyl chloride (PVC), polypropylene (PP), polystyrene (PS)], paper wastes [cardboard (CB), hygienic paper (HP), packaging paper (PK)], and yard wastes [pine wood branches (BR), leaves (LV) and grass (GR)]. A mixture (MX) between polypropylene, cardboard and branches at a mass ratio 1:1:1 was also prepared. Feedstocks were cut down into small pieces using a Rockwell mill and a chipper for PVC and branches and milled to a 2 mm particle size using a cryogenic grinder (Retsch SM 100).

A representative sample of each material was obtained using the standard method of coning and quartering (SABS method). The particle size distribution was determined using a Retsch sieve shaker operating for 10 minutes. Samples of particle size between 250 µm and 1 mm were used in the TGA experiments.

2.2 Analyses

Proximate analysis of feedstocks was carried out in accordance to the ASTM E1131 by means of a Mettler Toledo TGA/DSC1 thermogravimetric analyser. Samples were loaded in 900 µL alumina crucibles and were heated under a N_2 (99.999% Baseline 5.0, Afrox) flow of 80 mL/min at a heating rate of 50°C/min from 30°C to 110°C, following which an isothermal region was maintained for 30 s. The heating rate was then increased to 100°C/min until a temperature of

900°C was reached after which a second isothermal region was hold for 5 minutes. Finally, the atmosphere was changed from N_2 to O_2 (99.998% Baseline 4.8, Afrox), which flow rate was 80 mL/min for a further 5 minutes, to allow for complete combustion and determination of the ash content.

Ultimate analysis was carried out using a LECO TruSpec Micro Elemental Analyser where the amount of elemental carbon, hydrogen, nitrogen and sulphur present in each component was determined. The oxygen was calculated by difference. The higher heating value (HHV) of the feedstock was determined by means of an Eco cal2K bomb calorimeter. However, no calorific value could be obtained for PVC as the release of large amount of hydrochloric acid during its combustion is potentially corrosive. The results are presented in Table 1.

2.3 TGA-MS experiments

The thermal decomposition of individual components in MSW and their mixture was carried out in a Mettler Toledo TGA/DSC 1 analyser. Each sample (10-20 mg) was placed in a 70 µL alumina crucible and placed into the furnace where it was heated from 25°C to 1000°C at heating rate 20°C/min. The mass used varied between the samples since their densities were different. Low sample masses and low heating rate were chosen so as to reduce the occurrence of secondary vapour solid interactions and the effect of mass and heat transfer [23]. Blank runs were carried out to determine the effect of buoyancy on the experiments following which the TGA curves were corrected. Pyrolysis and combustion experiments were carried out using Argon (99.999% baseline 5.0, Afrox) and air (21% O_2/79%N_2, Afrox) respectively, at a flow rate 50 mL/min, with a hold time of 5 minutes before the start of the reaction, to ensure identical temperature distributions and thermal equilibrium of the samples at the start of the experiments. Weight loss measurements of the samples were recorded every 0.7 seconds. TGA experiments

were carried out in duplicate to confirm the reproducibility of the results. Data obtained from the TGA were interpreted and manipulated using the STARe-Evaluation software version 13.0 supplied by AKTS.

Volatile products were analysed by a mass spectrometry (MS) coupled to the TGA. A representative portion of the evolved gas components from the TG analyser was fed to a Pfeiffer Vacuum Thermostar GSD320 Gas Analysis System mass spectrometer through a well insulated 5m x 150µm fused silica capillary heated to 200°C. The input gas was ionised by a bombardment of electrons under positive electron impact ionization energy of 70eV. Cations were separated by a quadruple mass filter and reached a SEM MS detector. The subsequent mass spectrum provides a fingerprint of the complex vapours. Preliminary sensitivity and linearity tests using $CaCO_3$ standard were carried out to avoid any saturation of the detector and confirming the position of the capillary at the furnace exit.

In order to select the relevant molecular ions to track during the degradation, a preliminary-MS scan of the overall volatiles was applied to screen all ionic species in the range of 1 to 300 amu emitted by each sample recorded over 42 cycles. After comparison of the scans with literature [12, 18, 24] a list of 8 common fragments of the most intense ($I > 10^{-12}$ A) fragments (Supplementary data S1) were chosen. The intensity of the signal was normalised to the sample size and to the carrier gas ion (m/z 40) in order to have a comparable ion current across different stages and between different samples and to eliminate systematic instrumental errors.

The sensitivity and linearity of the MS detector was checked by pyrolyzing four different sample weights of PVC (5, 10, 15 and 20 mg) under dynamic regime at 20°C/min with a flow of 50 mL/min of Argon (99.999% baseline 5.0, Afrox). The plot of ion peak areas versus the initial masses of PVC introduced (Supplementary data S2) displayed a linear trend ($R^2 = 0.9884$)

159 indicating that the MS was sensitive enough with low sample masses and that a direct
160 relationship between the peak area and the sample mass could be used.
161 The effective activation energy as a function of conversion was evaluated for the samples and
162 mixture using the popular isoconversional analysis, Friedman's method. The samples were
163 heated from 25 to 1000°C using four heating rates (10, 20, 30 and 50°C/min) under both
164 pyrolysis and combustion conditions as described above. Although these heating rates appear to
165 be too high according ICTAC kinetics committee recommendations [25] to insure the kinetic
166 regime, the main objective of this study was to demonstrate that the TGA-MS method is an
167 adequate technique to semi-quantify synergistic events during the devolatilization of complex
168 polymers by combining devolatilization rates (dα/dt) and relative areas of MS peaks. All
169 resulting weight loss using TGA and their corresponding rate obtained from DTG curves at
170 different temperatures were treated using the Advanced Thermal Kinetics Software (AKTS
171 version 3.18). The E_α-dependency curves versus the extent of conversion were obtained using the
172 Friedman's method as described in detail by Aboyade *et al*. [26]. The equation used for the
173 determination of the apparent activation energy is given as:

174 $$\ln(\beta(d\alpha/dt)) = \ln[A.f(\propto)] - E/RT \qquad (1)$$

175 Where α is the conversion fraction, β is the heating rate, f(α) is the reaction model, A is the
176 Arrhenius pre-exponential factor and E the activation energy. A plot of ln(β (dα/dt)) against 1/T
177 for values obtained for different heating rates (β) at the same conversion (α) results in lines. The
178 E_α-dependency analysis has been proven to be a powerful tool to describe key features of thermal
179 conversions [27].

180 **3. Results and Discussion**

181 *3.1 Weight loss profiles of MSW during pyrolysis and combustion*

3.1.1 For individual materials

Each material was exposed to inert and oxidative thermal treatments and the main degradation stages are illustrated in Figures 1 and 2. Tables 2 and 3 summarise the main characteristics of TGA and DTG curves such as the temperature range in which the degradation took place, the temperature at which the maximal rate of loss weight occurred and the final percentage of solid residue. All materials except PVC and PK were pyrolysed in one stage (Figure 1). The pyrolysis degradation of PVC occurred in two distinct steps with peaks observed at 309°C and 450°C on the DTG curve which are in line with previous research on the pyrolytic behaviour of PVC [28]. The other two plastics PP and PS decomposed in a narrow range of temperature (Figure 1 and Table 2). Both plastics containing a high VM content (Table 1) presented similar pyrolysis trends with the fastest rates of weight loss (Table 2). This single stage degradation can be explained by the very homogeneous structure of plastics as mentioned by Bockhorn *et al.* [29]; with PP and PS's degradation occurring through the same radical chain mechanism, initiating via random scission followed by radical transfer. Hence the difference in the TG curves of PVC and the other two plastics can be attributed to the different macromolecular structure and pyrolysis mechanisms. The remaining solid residue for plastics (Table 2), as indicated by the presence of ash content (Table 1) is mainly due to the presence of additives, with fibre glass being the most common [30].

In the case of yard and paper wastes, the weight loss occurring below 100 °C is attributed to the loss of moisture [31]. Subsequent to dehydration, the degradation of the components in lignocelluloses (BR, LV, GR) with the lowest thermal stability started at the lowest temperatures, which corresponded to the typical degradation temperature range of hemicelluloses (160-360°C) [32]. Cellulosic-based (CB, HP) wastes started to degrade at a slightly higher temperature (210-

230°C), which corresponded to the reported temperature range of cellulose degradation (i.e., 240-390°C) [32]. The lignocellulosic-based (BR, LV, GR) materials presented broader degradation range (Figure 1) which was characteristic of the decomposition of lignin reported over a wide temperature range (180-900°C) [32] and to their higher FC content (Table 1). Brebu and Vasile [33], further attributed the broad temperature range for the thermal degradation of lignin to differences in thermal stabilities of the various oxygenated functional groups present in lignin. A change in the slope above 500°C for the lignocellulosic-based (BR, LV, GR) materials shows a slower rate of weight loss (Table 2), corresponding to a combination of the end of cellulose degradation and the start of secondary degradation of heavier volatiles and char formation process [31]. The latter restricts the mass transport at the solid/gas interface and hence slows down the rate of escape of the volatized gases [31]. On the other hand, PK paper's degradation pathway differed from the other cellulosic-based materials with two distinct peaks observed on the DTG curve at 362°C and 486°C, respectively. A small shoulder peak was also observed at 690°C. Similarly to HP and CB, the first stage of degradation between 250°C and 400°C corresponded to the degradation of cellulose. Skreiberg et al. [10] reported that the second stage (400-510°C) was a result of the degradation of $CaCO_3$ to CaO and CO_2. Calcium carbonate is often used as additives in these types of paper. A further thermal degradation above 500°C indicated the existence of more stable molecules or intermediates, inert below this temperature. Analyzing the width of the temperature range in which pyrolysis takes place for the different samples, it can be seen that the 9 MSW components can be put into the following order: PS, PP, BR, LV, PVC, HP, CB, GR and finally PK. PP, PS and BR had completed their thermal degradation by 500°C. The first three components are also the materials with the lowest ash content (Table 1). PK and GR, containing the highest ash content, continued to lose weight

above 600°C and were the most difficult to break down. The lower DTG peak observed for grasses was also reported in other studies [13] and was explained by the higher ash content of GR (Table 1) and the difference in the composition of ash.

The TGA and DTG curves of the combustion of the different components are presented in Figure 2. The DTG curves for all lignocellulosic-based materials (BR, LV, GR) were practically identical (Figure 2). The first degradation stage was in the range of 200-380°C and could be attributed to the breakdown of hemicelluloses and cellulose [32] up to 300°C. The second combustion-degradation stage (370-550°C), which was not clearly observed during pyrolysis, corresponded to the degradation of lignin although most probably due to the oxidation of char [34]. In most cases, the combustion of the feedstocks occurred at lower temperatures than pyrolysis (Table 3 and Supplementary data S3 for direct comparison of DTG curves). In particular for the lignocellulosic-based (BR and LV) and cellulosic based (CB, HP, PK) feedstocks, the rate of combustion (Table 3) was faster than the rate of pyrolysis (Table 2) at one exception for the grass, which displayed the lowest O content but also the highest ash content (Table 1). An increase in the content of oxygen and fixed carbon was thus beneficial to the rate of combustion. These oxidation conditions also facilitated the devolatilization of inorganics for all of the individual components considered, resulting in a lower weight fraction of residual solids after processing (Table 3). Furthermore, the combustion of lignocellulosic-based materials presents more stages of degradation than their pyrolysis degradation (Supplementary data S3). Similarly to pyrolysis, the combustion of plastic materials, PP and PS, occurred in a single stage but at lower temperatures (260-425°C). The absence of the second combustion stage indicated that no char was formed during the first stage of combustion, since these two plastics had a high VM content (Table 1). In the case of the combustion of PVC, a three staged degradation was

observed indicating the formation of char and its combustion in the last stage at high temperature of 610°C (Figure 2). Once again, the cellulosic-based material PK presented three-stage degradation under oxidative atmosphere. After a first volatilization at 335°C and the combined combustion of lignin and char (425°C), a third stage at 672°C was observed and could be attributed to the decomposition of calcium carbonate to calcium oxide and carbon dioxide [10].

3.1.2 For the mixture

The mixture consisted of one material from each feedstock group (i.e., lignocellulosic, cellulosic and plastic-based materials), PP, CB and BR. This preparation was subjected to pyrolysis and combustion under 20°C/min and main results are summarized in Figure 3. Under pyrolysis, the mixture was devolatilized in two distinct stages centred at 375 and 481°C (Table 2), with the former peak attributed to both devolatilization of hemicelluloses and cellulose fractions from lignocellulosic and cellulosic-based materials, while the latter mainly to PP devolatilization with minor contributions of lignin degradation, present in CB and BR (Table 2). Similar observations were made during the thermal degradation of MSW under inert conditions, which were attributed to the successive contributions of primary decomposition and secondary reactions [35].

Two stages of decomposition were detected during combustion (Figure 3) of the mixture. The two combustion stages overlapped to a greater extent when compared to the DTG curve of pyrolysis. Larger extents of volatile release, occurring at lower temperatures, were observed for combustion of the mixture, compared to pyrolysis (Tables 2 and 3), as was also observed with combustion/pyrolysis of single components. Significant weight loss of 88% was observed during the first combustion stage (225-400°C), associated with the decomposition of all the three components in the mixture (Table 3). A relatively weak and narrow peak (425°C) was observed in the second stage corresponding mostly to the oxidation of char and slow degradation of lignin.

The rate of devolatilization for the first peak was higher during combustion while the second peak was higher during pyrolysis.

3.1.3 Analysis of synergistic interactions during MSW mixture pyrolysis and combustion

The degradation of lignocellulosic-based and plastic materials occur through different types of mechanisms which can give rise to synergies. Usually lignocellulosic-based materials degrade through a series of different endothermic and exothermic reactions involving ionic/non-ionic reactions [36] while plastic degradation has been reported to occur through radical mechanism. In order to investigate the synergistic behaviour between the lignocellulosic-based and plastic materials in the mixture, theoretical DTG curves were also calculated as the sum of the weight loss rate contributions from BR, CB and PP fractions obtained under same conditions as shown in Figure 4. It was then assumed that there is no interaction between the different materials within the mixture. The predicted DTG curve was obtained using an additive equation (2):

$$Y = (x_c Y_c + x_b Y_b + x_p Y_p)/100 \qquad (2)$$

where Y refers to the predicted weight loss rate for the blended sample, Y_b is the observed weight loss rate at 100% BR, x_b is the fraction (%) of BR in the blend sample, Y_c is the observed weight loss rate at 100% CB, x_c is the fraction (%) of CB in the blend sample, Y_p is the observed weight loss rate at 100% PP and x_p is the fraction (%) of PP in the blend sample.

Under pyrolytic conditions, from the first peak at 375˚C, the reaction is slower than the calculated results showing some interactions between BR and CB, which is known to decompose in this temperature range. A slight shift of the second peak to higher temperatures could be observed. Synergistic effects were more evident for combustion of MX. The two expected peaks at 340˚C (BR and CB) and 380˚C (PP) have merged to produce one single peak at 348˚C. The

296 synergistic behaviour for the mixture under combustion conditions occurred over the temperature
297 range from 260°C to 515°C.
298 To further discuss on the extent of the synergistic effect during the pyrolysis and combustion of
299 the mixture, the difference of weight loss, ΔW (%), was calculated using equation (3).

300 $$\Delta W = W_{mix} - \left(x_b W_b + x_c W_c + x_p W_p\right) \quad (3)$$

301 Where W_{mix} is the experimental value from the TG curve of the mixture and W_b, W_c and W_p are
302 the weight losses from the TG curves of 100% BR, CB and PP. Figure 5 shows the plots of the
303 synergistic effects for the pyrolysis and combustion of MX. Negative values show a synergistic
304 effect towards the formation of char while positive values indicate synergistic effect during co-
305 pyrolysis and co-combustion for the formation of volatiles. For pyrolytic degradation, in the
306 temperature range of 25-330°C, a positive deviation of around 1.5% was observed indicating that
307 a minimum interaction between CB and BR occurred with a slightly higher release of volatiles
308 than expected. Between 330-500°C, two peaks can be observed on the curve that can be related
309 to negative synergistic effects. The first peak at 400°C, corresponding to the beginning of the
310 thermal degradation of PP, indicated that reactions between pyrolysis intermediates evolved from
311 the decomposition of the mixture led to the formation of more thermally stable compounds than
312 in the case of the single feedstock. At this temperature, the main degradation zone for PP, BR
313 and CB overlaps. The presence of intermediate species evolved during the degradation of BR
314 and CB could affects the degradation of PP by abstracting free hydrogen produced during
315 pyrolysis (Hydrogen transfer effect). Therefore the first negative synergistic peak observed is
316 most probably due to the abstraction of hydrogen by reactive species (e.g., radicals) which are
317 not available anymore to participate further in depolymerisation reactions. The second peak, with
318 a maximum of -4% at 480°C is coincident with the DTG peak temperature of degradation of PP

(Table 2). The volatile matter content of PP (Table 1) is much greater than that of BR and CB. At this temperature (480°C), during the degradation of MX, a large quantity and wide variety of volatiles was released from PP in a very short time period (Figure 6). Some of the volatiles may have been trapped in the particles' voids or condensed on BR, CB and PP particles' surface preventing the volatiles to be released. Further increase in temperature (>500°C) resulting in an inner pressure of the particles of BR, CB and PP was then beneficial for the formation and release of volatiles. Also, the negative synergistic effect due to the abstraction of hydrogens reported earlier at lower temperature is reduced since the degradation of PP should be completed by 500°C (Table 2). Positive deviation of around 3% was therefore observed and consistent over the whole conversion suggesting that interactions between reactive volatiles and/or between volatiles/solid promoted devolatilization reactions or inhibited reactions such as re-condensation and char formation. Past work on co-pyrolysis of plastic and biomass suggested that the formation of reactive radicals from PP could have catalyzed the decomposition of lignin producing more volatiles than expected towards the end of the degradation [37]. To further analyse the extent of synergistic effect, the root mean square (RMS) value was used. This method used in previous research allows the determination of the error between the measured and predicted values [22]. The RMS value of the deviation between the measured and calculated value was 2.38 which suggest that there were indeed synergistic effects during the co-pyrolysis of BR, CB and PP resulting in an overall less residual char.

During combustion, no difference in weight loss was observed ($\Delta W<0.6\%$) below 250°C. In the temperature range of 260-500°C, large and positive deviations in weight loss was obtained with two peaks occurring at 340 and 370°C. The first synergistic peak with a maximum of 9.2%, was coincident to the peak DTG for both degradations of BR and CB (Table 3) and the early stage of

PP degradation, which indicates that significant synergistic mechanisms promoting the devolatilization of solid occurred. Contrary to pyrolysis, the formation of free hydrogen radicals from PP is significantly reduced in the presence of oxygen. Therefore positive deviations observed could be related to the formation of steam, which could promote the further cracking of char from BR and CB leading to the formation of more volatiles. The second peak with a maximum of 14%, occurred at the critical temperature where PP degraded (Table 3) together with the second stage of degradation of individual lignocellulosic components, BR and CB. Radicals formed during the degradation of PP contributed to the formation of volatiles from BR and CB; thus suggesting that the nature of volatiles produced under oxidative atmosphere is more reactive. Above 500°C, negligible and positive deviations ($\Delta W<1\%$) were depicted (Figure 5). A RMS value of 3.37 for the ΔW was obtained which was higher than that obtained during pyrolysis. The RMS values indicated that the consequences related to the synergistic effects during the co-thermal conversion of BR, CB and PP yielded to smaller solid residue.

3.2 Evolved gas analysis during MSW pyrolysis and combustion

3.2.1 For individual materials – common fragments

The composition of gaseous products from the pyrolysis and combustion of individual components were analysed by online MS coupled to TGA. Figures 6 and 7 show the evolution of the six common fragments under pyrolytic and combustive conditions respectively. The structural formula of PVC, PP and PS are -[CH_2-CHCL]n-, -[CH_2-$CHCH_3$]n- and –[CH_2-CHC_6H_6]n- respectively. Since no oxygen is present in the structure of these materials, in theory it suggests that H_2O, CO and CO_2 should be absent in gaseous products obtained from their pyrolysis. Hence, the evolution profiles of H_2O, CO and CO_2 for PVC, PP and PS were not considered in Figure 6(a, b and c).When comparing the relative abundance of some selected

molecular ions (i.e. H_2, CH_4, H_2O, C_xH_y, CO and CO_2) common to all feedstocks , H_2, CH_4 and other hydrocarbons (HCs) were found to be released more abundantly under pyrolysis conditions, while H_2O, CO and CO_2 presented the highest intensities during combustion.

H_2O in gaseous products

H_2O release characterized by molecular ion fragment 18 amu, was released at several stages during the pyrolysis of natural polymers. Figures 6d-h revealed the presence of two peaks for H_2O during the thermal degradation of yard and paper wastes. The first peak below 200°C can be related to the first peak observed on the DTG curves of ligno-cellulosic based materials (Figure 1b) which corresponded to the release of moisture. The second peak, which occurred in the thermal degradation range of cellulose, was more pronounced for paper wastes (CB, HP and PK) and attributed to their higher cellulosic content when compared to those of yard wastes. The peak observed in the pyrolysis stage can be mainly ascribed to the release of intra molecules of water [9] from the hydroxyl group present in the structure of cellulose and to the release of hydroxyl groups during the degradation of higher molecular weight molecules [38].

Under combustive conditions, the recurrent record of higher intensities of H_2O^+ ions for PP and PS indicated that the oxidation of HCs present in plastic is an important mechanistic feature. PP displayed the highest intensity for the release of H_2O during combustion which is consistent with the high hydrogen content of PP (Table 1). The three MS peaks of H_2O observed during the combustion of PVC were found in good agreement with its DTG profile (Figure 2b). The release of H_2O during combustion of lignocellulosic-based materials (BR, LV, GR, CB, HP and PK) occurred in two main steps. Similarly to pyrolysis, the release of water at low temperature could correspond to dehydration. The second peak of H_2O may be attributed to the degradation of

glycosyl units present in cellulose [39] and most probably due to the oxidation of HC's released in that temperature range (200-500°C).

CO_2/CO in gaseous products

During pyrolysis, the non-condensable, CO (m/z 28) and CO_2 (m/z 44), evolved over the whole temperature range up to 600°C (Figures 6d-h). Higher proportions of CO_2 during the degradation of lignocellulosic-materials (BR, LV, GR) were detected while more CO was released during the degradation of cellulosic-based materials (CB, HP, PK). The formation of CO_2 is believed to be a consequence of the degradation of carbonyl (C=O) and carboxyl groups (COOH) present in hemicelluloses and cellulose and the product CO is the result of the scission of ether bonds (R-O-R') [40] indicating that ether groups are more dominant in paper wastes than yard wastes. At higher pyrolysis temperatures (>600°C), peaks of CO and CO_2 could be observed for paper wastes suggesting self-gasification according to equation (4) [18] and also the decomposition of calcium carbonates (equation (5)) present in paper wastes [41].

Stronger magnitude of both ions signal was observed for all the waste components burnt. Highest peaks were exhibited by PP and PS at 340°C and 420°C, respectively as the rich carbon content of the plastics (Table 1) were oxidised to CO and CO_2 in presence of air.

$$C + H_2O \rightarrow CO + H_2 \qquad (4)$$

$$CaCO_3 \rightarrow CaO + CO_2 \qquad (5)$$

H_2 in gaseous products

It is widely accepted that H_2 is mainly produced from the cracking of HCs and their subsequent degradation. Figure 6 revealed the presence of H_2 from the pyrolytic degradation of all the nine components. At higher temperatures (600-1000°C), the concentration of H_2 increased considerably for PVC, yard and paper wastes during pyrolysis. Similar observations were made

for CO (m/z 28) where H_2 is being produced following equation (4). Secondary cracking of higher molecular weight compounds and secondary pyrolysis of char residue contributed to the release of H_2 at elevated temperatures. The change in atmosphere from argon to air caused a high decrease in the intensity of H_2^+ ions, which could be attributed to the formation of water. Compared to the signals of the other light gases (CO, CO_2 and H_2O), the signal for H_2 was considered negligible in Figure 7.

C_xH_y in gaseous products

The fragment ions of m/z 16 (CH_4^+) and m/z 26 ($C_2H_2^+$) are mainly representative of the evolution of HCs. The intensity of the fragments for CH_4 was higher in most cases showing the cracking and evolution of lighter molecular gases. A single narrow peak for both fragments could be observed for PP and PS in the degradation stage at around 480˚C. Higher concentrations in ions were observed in the second stage of devolatilization of PVC as HCs are formed after the elimination of chlorine in the first stage and were subsequently degraded at higher temperatures during the second stage. For cellulosic-based materials (BR, LV, GR, CB HP and PK), the first peak shows the production of CH_4 mainly comes from the cracking of methyl and methylene groups present in hemicelluloses and cellulose and the second peak originates from the degradation of lignin.

In the presence of oxygen, HCs were oxidised to H_2O and CO_2 causing a significant decrease in the intensity of m/z 16 and m/z 26 (Figure 7). The intensity of m/z 16 was however higher than expected and attributed to the amount of O_2 in air.

HCN/NH_3 in gaseous products

The evolution of m/z 16 and m/z 26 are affected by the presence of NH_3 and HCN, respectively [24]. However, volatile nitrogenous gaseous compounds such as HCN and NH_3, are known to be

present in significantly low concentrations in waste materials [42, 43]. The nitrogen content of the different components in this study varied between 0 to 3% (Table 1), with plastic wastes having negligible nitrogen content and GR having the highest. Giuntoli et al. [44] detected low amounts of NH_3 and HCN compared to the levels of other volatile species during the pyrolysis of biomass residues. The gas analysis in another study [35] did not reveal the presence of NH_3 and HCN. To conclude, the peaks at m/z 16 and m/z 26 could be associated to the simultaneous release of NH_3 and HCN and mainly HCs in the case of cellulosic-based components; thus illustrating some limitations in the use of hard ionization source with mass spectrometry. Higher intensity of signals attributed to H_2, CH_4 and HCs and lower intensity for CO, CO_2 and H_2O signals collected under pyrolytic conditions suggest that the gas released could have a higher specific energy than combustion gas.

3.2.2 For the mixture of PP, BR and CB

For the sake of comparison, the MS peak areas were normalized to the initial mass of each feedstock to better illustrate synergistic effect when mixing PP, BR and CB. Also, a calculated MS peak area for the mixture, MX_{calc}, was determined by summing the relative contribution of each single component (Table 4). The MS curve of the different fragments for MX under pyrolytic and combustive conditions is given in Figure 8.

H_2O in gaseous product of the mixture

Water (m/z 18) evolution up to 200°C was observed during both degradation conditions and was due to the free and physically bounded water in CB and BR. The relative area of the first peak for both combustion and pyrolysis was 0.06nsA/mg and was close to the relative area obtained from CB (0.063nsA/mg) and BR (0.020nsA/mg). A second peak was observed at around 380°C during pyrolytic degradation which corresponded mostly to the degradation of CB and BR. Both

456 calculated and experimental normalized areas, 0.0320 and 0.0328 nsA/mg respectively, were
457 found close; thus suggesting that external water did not participate to further chemical reactions.
458 Peaks of H_2O were absent during the second stage of degradation where mostly the
459 devolatilization of PP takes place.
460 With respect to the combustion of MX, a second peak at 370°C displayed an experimental
461 normalized area, 0.19 nsA/mg, slightly higher than the calculated value, 0.15 nsA/mg. In this
462 temperature range, positive deviations were observed (Figure 5) for the decomposition of MX
463 suggesting that synergistic effect should affect mainly secondary reactions such as the secondary
464 cracking of the char and oxidation of hydrocarbons. Hence a higher release of H_2O fragments
465 was observed.
466 *CO_2/CO in gaseous products of the mixture*
467 Under pyrolysis conditions, significant releases of CO and CO_2 were observed at 375°C, 475°C
468 and 700°C. The highest peaks observed in the first stage were related to the degradation of BR
469 and CB (Figure 6). Deviations between first stage experimental and calculated normalized areas
470 (Table 4) confirmed that at this temperature (375°), the release of CO_2 and CO was inhibited.
471 This result is in accordance to ΔW (Figure 5) where negative deviations were observed in this
472 temperature range (230-400°C). It corresponds to the start of the degradation of PP where due to
473 hydrogen transfer effects, the release of volatiles was slowed down. Similarly, for the second
474 peak (475°C), lower peak areas were obtained (Table 4) which can be related to the negative
475 synergies observed at this temperature (Figure 5). The peak for the second stage corresponds to
476 the DTG peak of PP and the high release of hydrocarbons from the structure of PP prohibited the
477 release of CO and CO_2 from lignocellulosic materials. Peaks observed at higher temperatures

were similar to those obtained for CB and BR (Figure 6) showing self-gasification and degradation of carbonates.

The intensity of the peaks was higher during combustion showing the oxidation of hydrocarbons as compared to pyrolytic conditions. The experimental areas of the peaks were higher than the contribution from each component in the sample and occurred at the temperature where high positive deviations were obtained (Figure 5) showing that CO and CO_2 were important products during combustion resulting from synergistic reactions.

H_2 in gaseous product of the mixture

The significant and gradual increase in H_2^+ ions observed for MX pyrolysis could be related to the cracking of heavy hydrocarbons also known as secondary reactions. An opposite trend was observed during combustion where the concentration of H_2^+ ions decreased constantly.

C_xH_y in gaseous product of the mixture

During pyrolysis of MX, 2 peaks were observed for m/z 16 (CH_4^+) and m/z 26 ($C_2H_2^+$) at about 380 and 500°C. The normalized area of the first peak was lower than the calculated area suggesting that the presence of PP inhibited the release of the volatile hydrocarbons from BR and CB as also observed as a negative synergistic effect at this temperature (Figure 5). The second peak displayed a larger area than expected (Table 4) confirming the high reactivity of PP's intermediates at higher temperature promoting the thermal degradation of heavy non-volatiles into CH_4 and C_2H_2 ions. At this temperature, positive deviations were also observed (Figure 5) which shows that the extent of devolatilization (ΔW) is in accordance to the MS peak areas.

It is worth noting that the release of ions during the combustion occurred in the same temperature range, 250-415°C, than pyrolysis. The experimental area value of 0.0099 nsA/mg appeared to be higher than the calculated one, 0.0005nsA/mg showing positive deviations.

3.3 E_α-dependency analysis for overall reactions and individual stages

In order to gain qualitative insights into the synergistic effects occurring during the blending of MSW components, the apparent activation energy (E_α) for the overall and single stages of PP, BR, CB and MX pyrolysis was determined and presented in Figure 9.

The E_α-dependency analysis for PP indicates that this latter remains quasi constant throughout the entire pyrolysis and combustion, and therefore the single degradation stage (Figures 1 and 2) can be associated to the single and averaged values of ~ 250 kJ/mol and 90 kJ/mol, respectively. Although the thermal degradation of PP during pyrolysis mainly involves the breaking of the C-C bonds whose energy bond is around 350 kJ/mol [27], a lower E_α was obtained for PP and can therefore be attributed to the presence of weak link sites [45]. The slight variations from the average value maybe related to the occurrence of various initiation mechanisms (e.g., breakage of head to head linkages, fractionation of vinyldene-end groups) and random scission [46]. Under oxidative conditions, the lower E_α values between 75-90 kJ/mol for PP indicated that oxygenated compounds may have favoured the thermal degradation pathways due to the presence of hydroperoxide radicals according to Vyazovkin and Sbirrazzuoli [27].

As expected, pyrolysis and combustion of the biomass (BR) underwent through more complex reactions mainly 2 main degradation stages. For BR pyrolysis, the initial average E_α values, 160 kJ/mol (Figure 9b) were found similar to those reported for the degradation of hemicelluloses, 107-164 kJ/mol [46]. An increase in E_α values to ~230 kJ/mol could mark the beginning of cellulose decomposition, which in general varies between 200 and 230 kJ/mol [46]. In the case of biomass combustion, these latter are usually associated to the devolatilization stage with average E_α values decreasing from 295 kJ/mol to 95 kJ/mol and to the char oxidation stage with a practically average value of around 150 kJ/mol. When considering the respective E_α-dependency

524 determined for each stage, the start of 2nd combustion stage requires less energy than the 1st
525 combustion stage. E_α during pyrolysis were higher than combustion showing a different
526 degradation mechanism occurring in air with reactions of lower activation energy.
527 The E_α during the initial degradation stage of cellulosic derived feedstock (CB) was lower than
528 that ascribed to the biomass-derived feedstock (BR) with average values of ~ 65 kJ/mol during
529 both pyrolysis and combustion. During pyrolysis of CB, an averaged E_α value of 200 kJ/mol was
530 obtained which corresponded to those of cellulose degradation [46]. The almost constant E_α
531 values (Figure 9c) confirmed the uniform energetic demand of cellulose degradation reactions.
532 For combustion, lower E_α of around 170 kJ/mol were obtained in the first stage of degradation as
533 compared to E_α of around 200 kJ/mol in the second stage. Similar to BR, E_α were lower during
534 combustion when compared to pyrolysis. The degradation of cellulose in air might therefore be
535 enhanced by molecular oxygens through radical interactions.
536 When the mixture was respectively exposed to inert and oxidative atmospheres (Figure 9d),
537 comparable key features in E_α-dependency were observed: both processes occurred in 2 main
538 stages with higher average E_α values for pyrolysis. However, slight deviations in E_α values from
539 those obtained for the single feedstocks were found. For example, the E_α values and the
540 noticeable decreasing trend of the E_α curve for the 1st degradation stage when α is increased is
541 almost equivalent to E_α-dependencies obtained for CB and BR. This result suggests that
542 mechanisms involved during 1st stage of MX pyrolysis are equivalent to those of cellulose-
543 derived feedstocks and can explain the absence of synergies mentioned in section 3.1.3. The
544 second stage of degradation of MX is mainly dominated by the degradation of PP. The E_α values
545 for the 2nd stage were higher than those for PP, BR and CB up to α=0.65 during pyrolysis (Figure
546 9d) thus indicating that intermediate species involved have a greater thermal stability. This

greater amount of energy required of around 300 kJ/mol instead of 250 kJ/mol, corresponds to the negative synergistic effects described earlier in the section 3.1.3 and is attributed to PP degradation. However, this energy penalty is compensated by the lowest energetic requirements for $\alpha > 0.7$ reaching 160 kJ/mol at $\alpha=0.9$. These lower $E\alpha$ values suggest that further degradations of PP eased the overall degradation mechanisms, which is in accordance with the positive synergistic effects described earlier in section 3.12. This lower activation energy and positive deviations were observed until the end of the second degradation stage. In the case of combustion, this positive impact of PP addition was even more significant with noticeable lowest E_α values for both degradation stages (Figure 9d), which was also corroborated by the extent of positive synergy effects (Table 4). Less energy is required during the combustion of MX as compared to the single components. Positive synergistic effects are indeed present during combustion of MX where the degradation mechanism occurs through a lower activation energy pathway. Similar to the single components, lower E_α was observed during combustion as compared to pyrolysis and hence indicating that the presence of oxygen indeed changes the degradation pathway with reaction of lower energies occurring.

4. Conclusions

Real time pyrolysis and combustion characteristics (i.e., solid conversion and release of volatiles) of nine components representative of current waste streams found in Mauritius and their mixture were investigated using a thermogravimetric analyser coupled to a mass spectrometer (TGA-MS). The mixture of MSW composed of lignocellulosic and plastic-based materials was degraded in two main stages under pyrolysis conditions while the combustion of the same mixture occurred in one main stage. Considering the differences between experimental and calculated results, it was found that both negative and positive synergistic effects were

present at different stages during pyrolysis. Negative synergistic effects observed in the 1st stage of pyrolysis between 330-550°C associated with higher E_α resulted in the formation of solid residue delaying the degradation of lignocellulosic materials. In this stage, the expected areas for the release of CH_4, CO and CO_2 were lower than experimental areas obtained showing that the release of the volatiles were slowed down. Above 500°C, increasing weight losses indicated that the decomposition of solid residues was favoured due to the presence of heterogeneous reactions of lower E_α between the char and reactive volatiles evolved from the degradation of PP. The difference between the value of the expected and experimental peak areas for the different volatiles tracked also confirmed the presence of positive synergies in this stage. Under oxidative atmosphere, only positive deviations up to 14% were recorded between 260-500°C; thus indicating that homogeneous interactions between volatiles enhanced the combustion of the mixture associated with lower E_α. This study confirms that the adopted experimental methodology based on TGA-MS is suitable for revealing the extent of synergistic reactions during co-pyrolysis and co-combustion.

Acknowledgement

We gratefully acknowledge Mauritius research council (MRC), University of Stellenbosch (International Office) and PAFROID program for financial support.

588 **References**

589 [1] P.Modak, Community-based Waste Management and Composting for Climate/Co-
590 benefits, Case of Bangladesh, The International Consultative Meeting on expanding
591 Waste Management Services in Developing Countries, 18-19 March, Tokyo, Japan
592 (2010).
593 [2] P. Gopee, M.D. Nowbuth, Y.B. Moonshiram, Evaluating the potential for recycling of
594 solid waste in Mauritius, 1st Internaltional Exergy, Life cycle assessment and
595 sustainability workshop and symposium proceedings, 4-6 June, Wisyros-Greece, (2009),
596 pp472-479
597 [3] A.M. Troschinetz, J.R. Mihelcic, Sustainable recycling of municipal solid waste in
598 developing countries, Waste Management 29 (2009) 915–923.
599 [4] R. Mohee, S. Rungasamy, M.A.Z, Bundhoo, Solid Waste Management in Mauritius, with
600 emphasis on the National Composting Plant, Journal of Institution of Engineers Mauritius
601 (2012) 67-73
602 [5] Z. Lai, X. Ma, Y. Tang, H. Lin, Thermogravimetric analysis of the thermal
603 decomposition of MSW in N2,CO2 and CO2/N2atmospheres, Fuel Process. Technol.
604 102 (2012) 18-23.
605 [6] A. Bosman, I. Vandereydt, D. Geysen, L. Helsen, The crucial role of Waste-to-Energy
606 technologies in enhanced landfill mining: a technology review, Journal of Cleaner
607 Production (2012) 1-14
608 [7] R. Mohee, Assessing the recovery potential of solid waste in Mauritius, Resources,
609 Conservation and Recycling, 36 (2002) 33–43.

610 [8] I. Velghe, R. Carleer, J. Yperman, S.Schmeurs, Study of the pyrolysis of municipal solid
611 waste, J. Anal. Appl. Pyrolysis 92 (2011) 366-375
612 [9] T. Karayildirim, J. Yanik, M. Yuksel, Y. Bochorn, Characterisation of products from
613 pyrolysis of waste sludges, Fuel 85 (2006) 1498-1508.
614 [10] A. Skreiberg, O. Skreiberg, J. Sandquist, L. Sorum, TGA and macro-TGA
615 characterisation of biomass fuels and fuel mixture, Fuel 90 (2011) 2182-2197.
616 [11] N. Tudorachi, A.P. Chiriac, TGA/FTIR/MS study on thermal decomposition of
617 poly(succinimide) and sodium poly(aspartate), Polym. Test. 30 (2011) 397–407.
618 [12] S. Singh, C. Wu, T. Williams, Pyrolysis of waste materials using TGA-MS and
619 TGA-FTIR as complementary characterisation techniques, J. Anal. Appl. Pyrolysis 94
620 (2012) 99-107.
621 [13] J. Heinkkinnen, J. Hordijk, W. Jong, H, Spliethoff, Thermogravimetry as a tool to
622 classify waste components to be used for energy production, J. Anal. Appl. Pyrolysis 71
623 (2004) 883–900.
624 [14] M. Muthuraman, T. Namioka, K. Yoshikawa, A comparative study on co-combustion
625 performance of municipal solid waste and Indonesian coal with high ash Indian coal: A
626 thermogravimetric analysis, Fuel Process. Technol. 91 (2010) 550–558.
627 [15] Z. Lai, X. Na. Y. Tang, H. Lin, A study on municipal solid waste combustion in N_2/O_2
628 and CO_2/O_2 atmosphere from perspective of TGA, Energy 36 (2011) 819-824.
629 [16] G. Skrodas, P. Grammelis, P. Basinas, M. Prokopidou, E. Kakaras, G.P.
630 Sakellaropoulos, A thermochemical conversion study on the combustion of residue
631 derived fuel, Water air soil pollution 9(2009) 151-157

[17] C.J. Gomez, E. Meszaros, E. Jakab, E. Velo, L. Puigjaner, Thermogravimetry/mass spectrometry study of woody residues and an herbaceous biomass crop using PCA techniques, J. Anal. Appl. Pyrolysis 80 (2005) 416-426.

[18] Y.F. Huang, W.H. Kuan, P.T. Chiwh, S.L. Lo, Pyrolysis of biomass by thermal analysis –mass spectrometry, Bioresource technology volume 102 (2011) 3527-3534.

[19] L. Tiikma, I. Johannes, H. Luik, A. Gregor, Synergy in the hydrothermal pyrolysis of oil shale/sawdust blends, J. Anal. Appl. Pyrolysis 117 (2016) 247-256.

[20] L. Zhou, Y. Wang, Q. Huang, J. Cai, Thermogravimetric characteristics and kinetics of plastic and biomass blends co-pyrolysis, Fuel Process. Technol. 87 (2006) 963-969.

[21] G. Wang, A. Li, Thermal decomposition and kinetics of mixtures of polylactic acid and biomass during co-pyrolysis, Chinese J. Chem, Eng. 16 (2008) 929-933.

[22] Z.Wu, S.Wang, J.Zhao, L.Chen, H.Meng, Synergistic effect on thermal behaviour during co-pyrolysis of lignocellulosic biomass model components blend with bituminous coal, Bioresource technology 169 (2014) 220-228.

[23] M.J. Antal, G. Varhegyi, Cellulose pyrolysis kinetics: the current state of knowledge, Industrial & Engineering, Chemistry Research 34 (1995) 703–717.

[24] NIST, 2013. NIST chemistry webBook. US secretary of commerce. Available from http://webbook.nist.gov/chemistry/

[25] S. Vyazovkin, A.K. Burnham, J.M. Criado, L.A. Perez-Maqueda, C. Popescu, N. Sbirrazzuoli, ICTAC Kinetics Committee recommendations for performing kinetic computations on thermal analysis data, Thermochimica Acta, 520 (2011) 1-19.

[26] A.O. Aboyade, T.J. Hugo, M. Carrier, E.L. Meyer, R. Stahl., J.H. Knoetze, J.F. Görgens, Non-isothermal kinetic analysis of the devolatilization of corn cobs and sugar cane bagasse in inert atmosphere, Thermochim. Acta 517 (2011) 81-89.

[27] S. Vyazovkin, N. Sbirrazzuoli, Isoconversional kinetic analysis of thermally stimulated processes in polymers, Macromol. Rapid. Commun.27 (2006) 1515-1532

[28] J. Blazevsca-Gilez, D. Spaseska, Formal kinetic analysis of PVC thermal degradation, Journal of the University of Chemical Technology and Metallurgy, 45(3) (2010), 251-254.

[29] H. Bockhorn, J. Hentschel, A. Hornung, U. Hornung, Environmental engineering: stepwise pyrolysis of plastic waste, Chem Eng Sci 54 (1999) 3043-3051.

[30] V.S. Loo, J. Koppejan, Handbook of biomass combustion and co-firing, UK, Earthscan (2002)

[31] P.R. Diaz, Z.H. Shemet, V.A. Lavrenko, V.A. Khristich, Studies on thermal decomposition and combustion mechanism of bagasse under non-isothermal conditions, Thermochim. Acta 93 (1985)349–352.

[32] G. Varhegyi, M.J. Antal, T. Szekely, P. Szabo, Kinetics of the thermal decomposition of cellulose, hemicellulose, and sugarcane bagasse, Energy&Fuels 3 (1989) 329–335.

[33] M. Brebu, C. Vasile, Thermal degradation of lignin – A review, Cellulose Chemistry and Technology 44 (9) (2010) 353-363.

[34] A.G. Barneto, J.J.A. CarmonaJ, E. Martin, J.D. Blanco, Kinetic models based in biomass components for the combustion and pyrolysis of sewage sludge and its compost , J. Anal. Appl. Pyrolysis 86 (1) (2009) 108–114.

675 [35] W.K. Buah, A.M. Cunlife, P.T. Williams, Characterisation of products from the
676 pyrolysis of municipal solid wastes, Process safety and Environmental 85 (2007) 450-
677 457.
678 [36] A. Dermidas, Pyrolysis mechanisms of biomass materials, Energy source part A 31 (2009)
679 1186-1193.
680 [37] M. Ahmaruzzaman, D.K. Sharma, Co-processing of petroleum vacuum residue with
681 plastics, coal and biomass and its synergistic effects, Energy & Fuels 21 (2) (2007) 891-
682 899.
683 [38] J. Adam, M. Blazso, E. Meszaros, M. Stocker, M.H. Nilsen, A. Bouzga, J.E. Hustad, M.
684 Gronli, G. Oye, Pyrolysis of biomass in the presence of A1-MCM-41 catalysts, Fuel 84
685 (2005) 1494–1502.
686 [39] D. Lopez-Gonzalez, M. Fernandez-Lopez, J.L. Valverde, L. Sanchez-Silva,
687 Thermogravimetric-mass spectrometric analysis on combustion of lignocellulosic
688 biomass, Bioresource Technology 143(2013) 562-574.
689 [40] K. Cheng, W.T. Winter, A.J. Stipanovic, A modulated-TGA approach to the kinetics of
690 lignocellulosic biomass pyrolysis/combustion. Polym. Degrad. Stab. 97(9) (2012) 1606-
691 1615.
692 [41] .A.J. Ridout, M. Carrier, J. Gorgens, Fast pyrolysis of low and high ash paper waste
693 sludge: Influence of reactor temperature and pellet size, J. Anal. Appl. Pyrolysis 111
694 (2015) 64-75.
695 [42] J.H. Ferasse, S. Chavez, P. Arlabosse, N. Dupuv, Chemometrics as a tool for analysis of
696 evolved gas during the thermal treatment of sewage sludge using coupled TG-FTIR,
697 Thermochim. Acta 404 (2003) 97–108.

[43] L. Tao, G. Zhao, J. Qian, Y. Qin, TG-FTIR characterisation of pyrolysis of waste mixtures of paint and tar slag, J. Hazard. Mater. 175 (2010) 754–761.

[44] J. Giuntoli, W. Jong, S. Arvelakis, H. Spliethoff, A.H.M. Verkooijen, Quantitative and Kinetic TG-FTIR study of biomass residue pyrolysis: dry distiller's grain with soluble (DDGS) and chicken manure, J. Anal. Appl. Pyrolysis 85 (2009) 301-312.

[45] J.D. Peterson, S. Vyazovkin, C.A. Wight, Kinetics of the thermal and thermo-oxidative degradation of polystyrene, polyethylene and polypropylene, Macromol.Chem.Phys., 202 (2001) 775–784.

[46] P. Grammelis, P. Basinas, A. Malliopoulou, G. Sakellaropoulos, Pyrolysis kinetics and combustion characteristics of waste recovered fuels, Fuel 88 (2009) 195-205.

Table 1
Standard fuel analysis

Sample	Proximate Analysis (wt% db)				Ultimate Analysis (wt% db)					HHV (MJ/kg)
	MC	VM	FC	Ash	C	H	O[a]	N	S	
PVC	0.02	88.95	8.67	2.36	38.8	5.14	53.61[b]	0.09	-	n.d
PP	0.00	99.85	0.00	0.15	85.03	14.8	0.00	0.00	0.00	42.80
PS	0.50	99.24	0.02	0.24	90.55	7.82	0.00	0.17	1.22	38.60

BR	0.71	79.80	17.27	2.22	45.35	5.96	44.55	0.22	1.70	21.43
LV	1.68	72.53	20.76	5.03	46.13	6.15	42.13	0.56	0.10	17.66
GR	1.77	61.27	14.86	22.10	32.65	4.95	35.24	3.07	1.99	20.64
CB	3.24	78.07	8.64	10.05	40.64	6.19	42.97	0.05	0.10	20.46
PK	3.40	78.38	7.43	11.79	42.6	6.41	37.08	0.21	1.91	22.75
HP	3.20	83.55	10.04	3.21	39.6	5.74	49.40	0.20	1.85	15.30

719 db- Dry Basis MC-Moisture content VM- Volatile matter FC-Fixed Carbon HHV- Higher Heating Value

720

721 [a] By difference

722 [b] It is Cl for PVC

723

724

Table 2

Characteristics of the TGA experiments of single components under pyrolytic conditions

Sample	Solid Residue at 1000°C (%)	DTG peak temperature (°C)	DTG max (1/s)	T_{onset} (°C)	Temperature Range (°C)
PVC	11.5	327, 495[a]	-0.0032, -0.0013[a]	296	240-400, 400-560
PP	2.8	479	-0.0099	454	370-500
PS	2.9	425	-0.0099	409	330-475
BR	18.7	375	-0.0025	320	201-500
LV	23.8	368	-0.0015	299	150-520
GR	25.5	330	-0.0019	274	160-600
PK	15.5	362, 486, 700[a]	-0.0030, -0.0017, -0.0003[a]	328	230-410, 410-540, 540-720
CB	16.7	370	-0.0039	333	230-600
HP	10.7	375	-0.0051	334	210-560
MX	9.84	375, 481	-0.02, -0.03	327	200-415, 415-525

[a] Several distinct peaks observed

Table 3

Characteristics of the TGA experiments of single components under combustion conditions

Sample	Solid residue at 1000°C (%)	DTG peak temperature (°C)	DTG max (1/s)	T_{onset} (°C)	Temperature Range (°C)
PVC	0.14	309, 450[a]	-0.0045, -0.0115[a]	295	225-375, 430-500, 500-690[a]
PP	1.19	380	-0.0058	348	260-400
PS	1.21	400	-0.0080	380	275-425
BR	1.67	335, 460[a]	-0.0039, -0.0007[a]	311	200-370, 370-520[a]
LV	4.00	230, 430[a]	-0.0021, -0.0014[a]	291	190-370, 370-550[a]
GR	9.85	295, 435[a]	-0.0017, -0.0014[a]	257	125-360, 360-545[a]
PK	8.78	335, 425, 690[a]	-0.0043, -0.0010, -0.0028[a]	312	280-380, 385-490, 500-715
CB	10.30	340, 420[a]	-0.0063, -0.0013[a]	327	210-375, 375-480[a]
HP	0.53	345, 435[a]	-0.0087, -0.0036[a]	328	260-385, 385-500[a]
MX	3.45	348, 425[a]	-0.04, -0.001	311	225-400, 400-470

[a] Several distinct peaks observed

Table 4

Relative areas of MS peaks for MX and pure components

	Pyrolysis									Combustion				
m/z	Degradation Stages													
	Stage 1 (nsA/mg)				Stage 2 (nsA/mg)					Stage 1 (nsA/mg)				
	BR	CB	MX_{calc}	MX_{exp}	BR	CB	PP	MX_{calc}	MX_{exp}	BR	CB	PP	MX_{calc}	MX_{exp}
16	0.0003	0.0017	0.0020	0.0010	-	-	0.0013	0.0013	0.0047	0.0030	0.0013	0.0030	0.0073	0.0096
18	0.0150	0.0170	0.0320	0.0328	-	-	-		-	0.0430	0.0270	0.0800	0.1500	0.1900
26	0.0003	0.0013	0.0016	0.0006	0.0001	-	0.0051	0.0052	0.0073	0.0002	0.0003	0.0027	0.0032	0.0039
28	0.0057	0.0122	0.0179	0.0153	0.0023	0.0008	-	0.0031	0.0026	0.0640	0.0770	0.0910	0.2320	0.2340
44	0.0107	0.0117	0.0224	0.0196	0.0014	-	-	0.0014	0.0007	0.0550	0.0610	0.0740	0.1900	0.2100

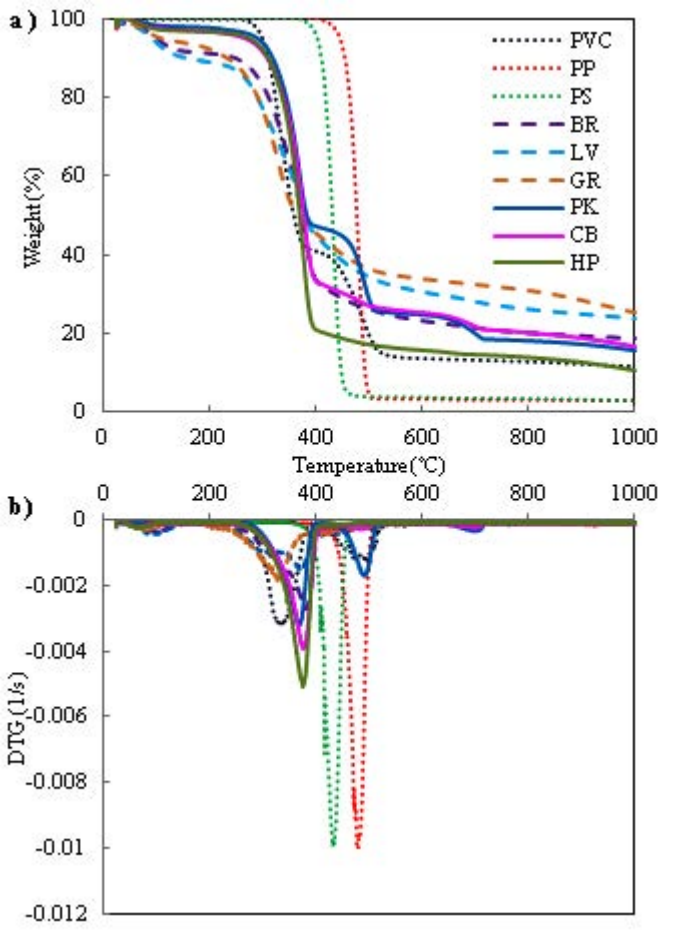
a)
Weight(%)
100
80
60
40
20
0
PVC
PP
PS
BR
LV
GR
PK
CB
HP
0
200
400
600
800
1000
Temperature(℃)
b)
DTG(1/s)
0
-0.002
-0.004
-0.006
-0.008
-0.01
-0.012

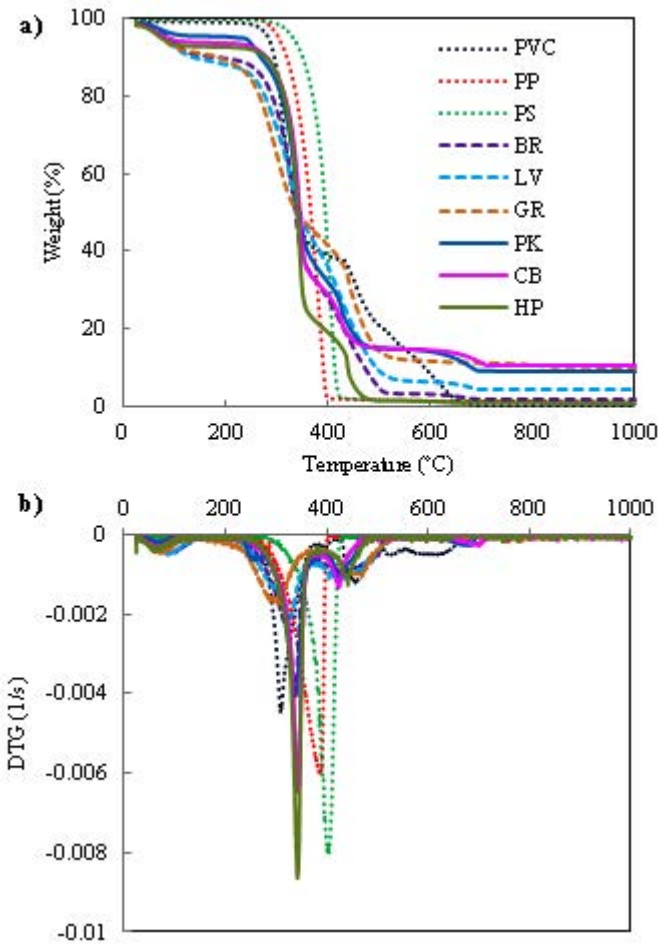
a)
Weight (%)
Temperature (°C)
PVC
PP
PS
BR
LV
GR
PK
CB
HP
b)
DTG (1/s)

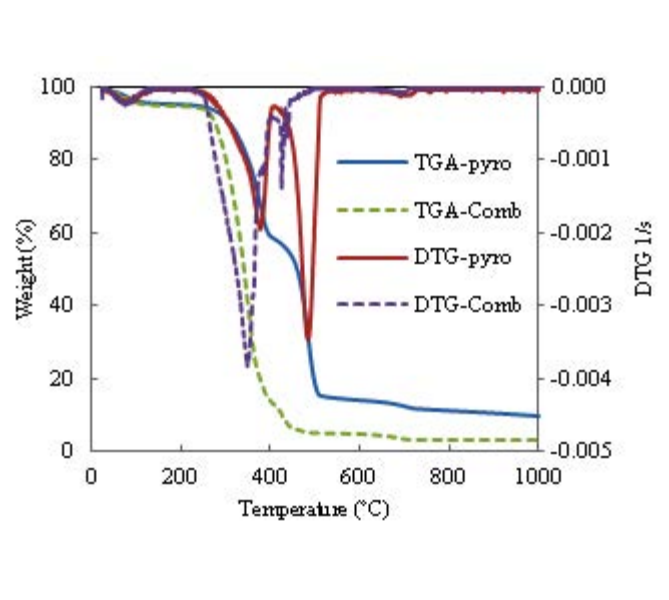
100
80
60
40
20
0
Weight (%)
0.000
-0.001
-0.002
-0.003
-0.004
-0.005
DTG 1/s
TGA-pyro
TGA-Comb
DTG-pyro
DTG-Comb
0
200
400
600
800
1000
Temperature (°C)

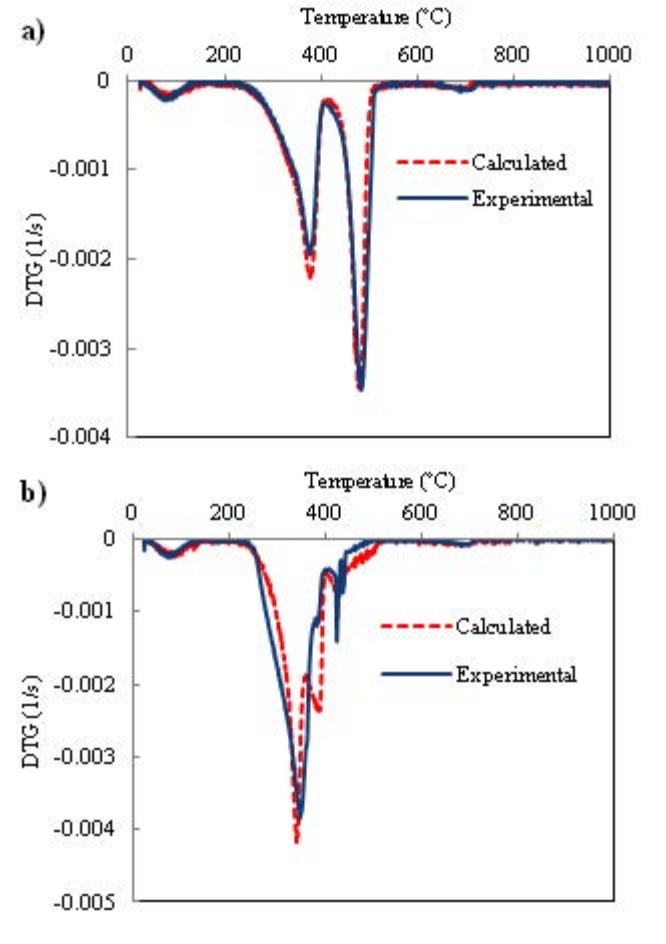
a)
Temperature (°C)
0
200
400
600
800
1000
0
-0.001
-0.002
-0.003
-0.004
DTG (1/s)
Calculated
Experimental
b)
Temperature (°C)
0
200
400
600
800
1000
0
-0.001
-0.002
-0.003
-0.004
-0.005
DTG (1/s)
Calculated
Experimental

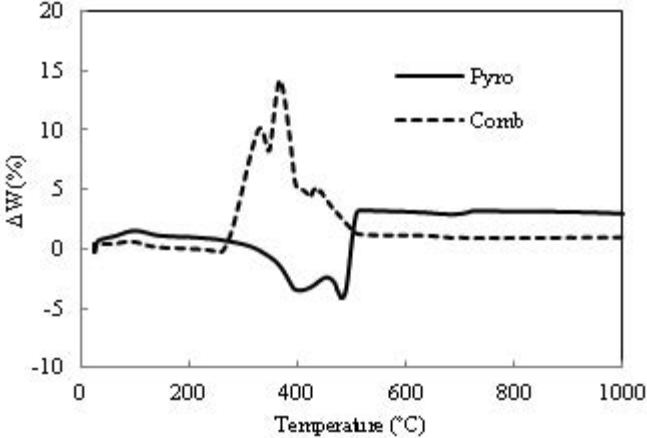
20
15
10
5
0
-5
-10
ΔW(%)
Pyro
Comb
0
200
400
600
800
1000
Temperature (°C)

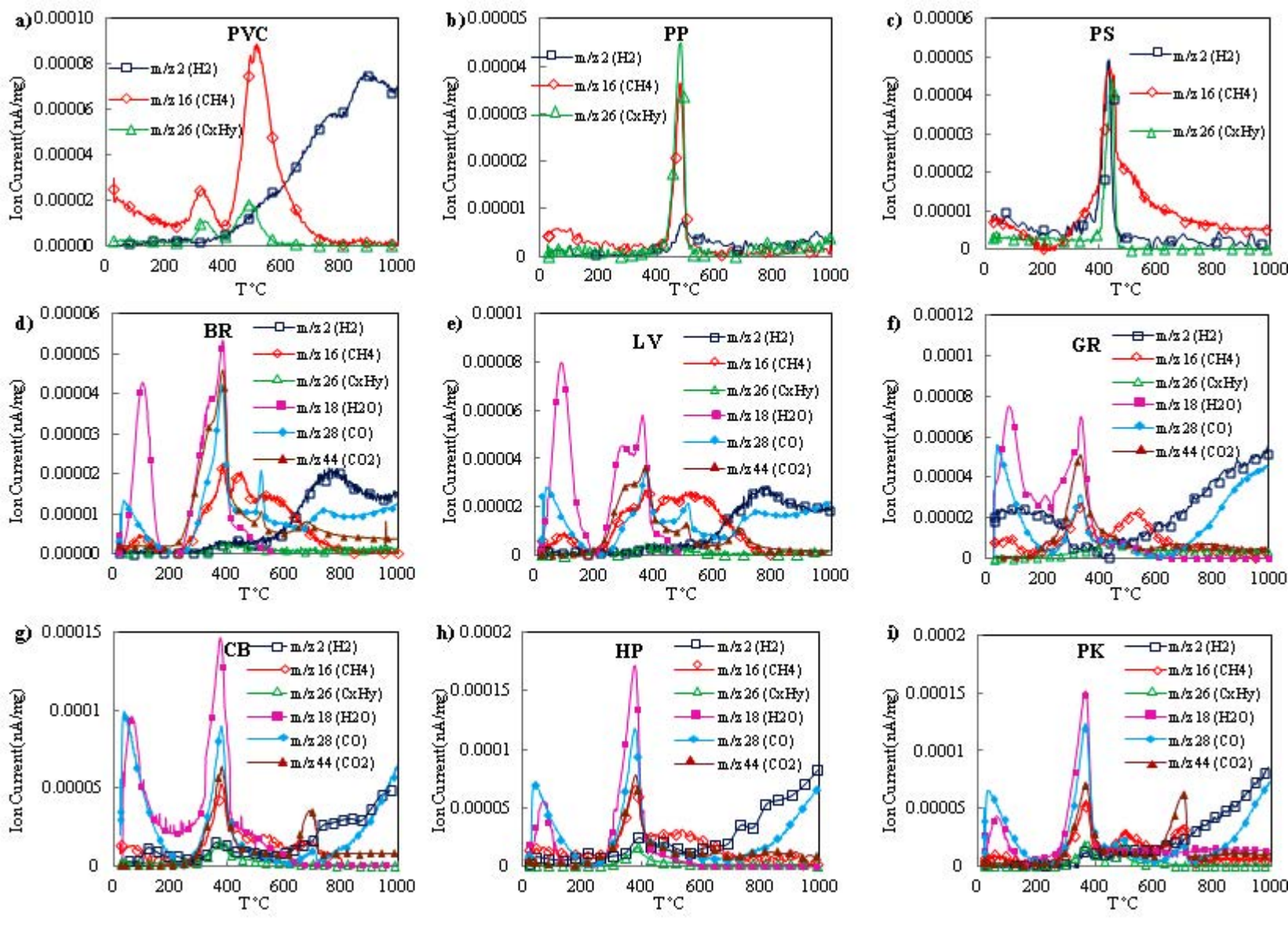
a)
PVC
b)
PP
c)
PS
d)
BR
e)
LV
f)
GR
g)
CB
h)
HP
i)
PK
m/z 2 (H2)
m/z 16 (CH4)
m/z 26 (CxHy)
m/z 18 (H2O)
m/z 28 (CO)
m/z 44 (CO2)
Ion Current(nA/mg)
T°C

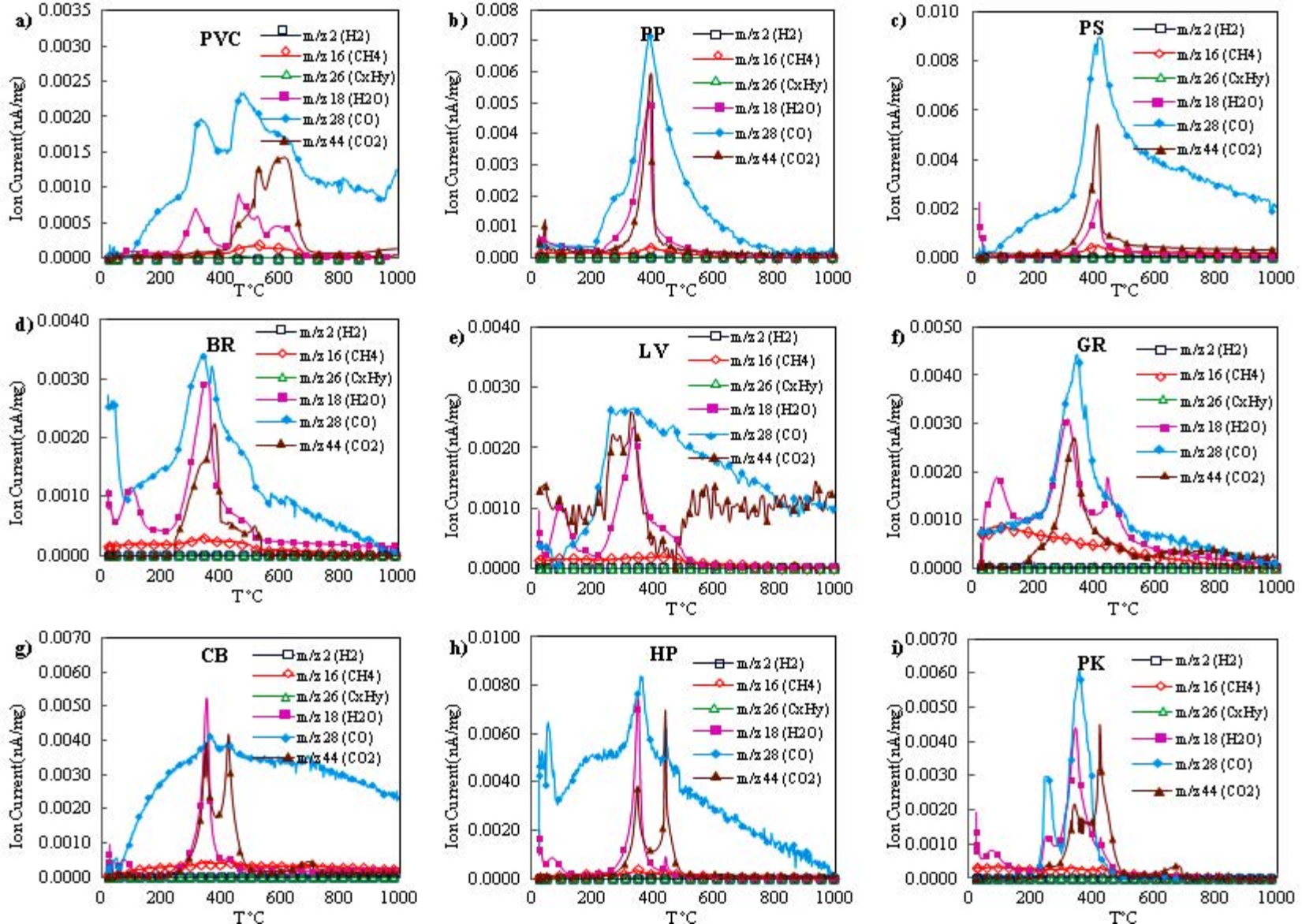
a)
PVC
b)
PP
c)
PS
d)
BR
e)
LV
f)
GR
g)
CB
h)
HP
i)
PK
m/z 2 (H2)
m/z 16 (CH4)
m/z 26 (CxHy)
m/z 18 (H2O)
m/z 28 (CO)
m/z 44 (CO2)
Ion Current(nA/mg)
T°C

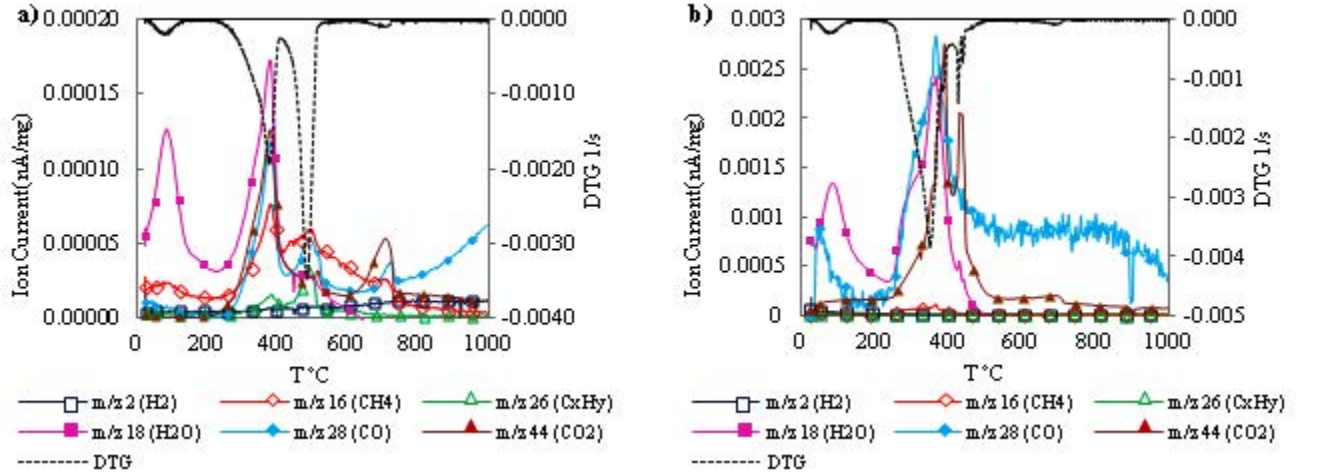
a)
b)
Ion Current(nA/mg)
DTG 1/s
T°C
m/z 2 (H2)
m/z 16 (CH4)
m/z 26 (CxHy)
m/z 18 (H2O)
m/z 28 (CO)
m/z 44 (CO2)
DTG

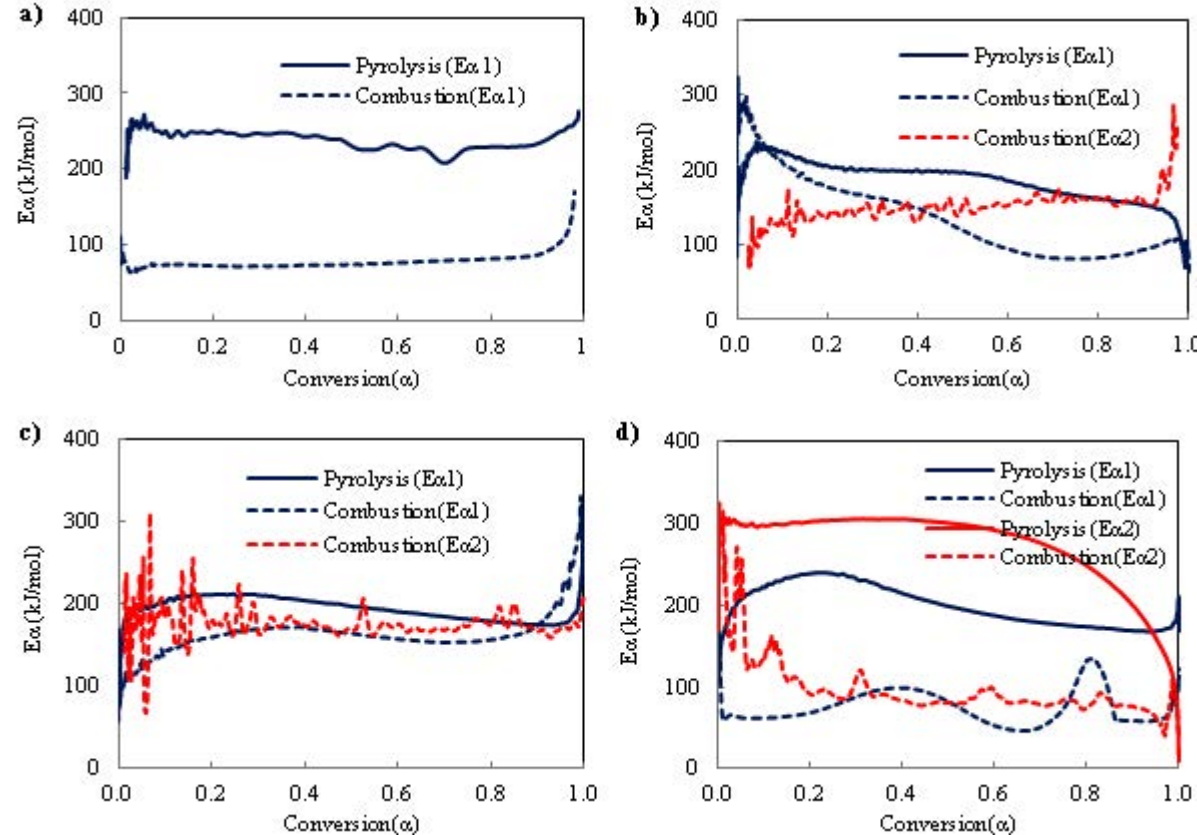
a)
Pyrolysis (Eα1)
Combustion(Eα1)
Eα (kJ/mol)
Conversion(α)
b)
Pyrolysis (Eα1)
Combustion(Eα1)
Combustion(Eα2)
Eα (kJ/mol)
Conversion(α)
c)
Pyrolysis (Eα1)
Combustion(Eα1)
Combustion(Eα2)
Eα (kJ/mol)
Conversion(α)
d)
Pyrolysis (Eα1)
Combustion(Eα1)
Pyrolysis (Eα2)
Combustion(Eα2)
Eα (kJ/mol)
Conversion(α)